Available online at www.eccomasproceedia.org
Eccomas Proceedia SMART (2023) 1623-1634

ECCOMAS
Proceedia

X ECCOMAS Thematic Conference on Smart Structures and Materials
SMART 2023
D.A. Saravanos, A. Benjeddou, N. Chrysochoidis and T. Theodosiou (Eds)

ADVANCEMENTS IN MONITORING OF TRIBOLOGICAL STRESS IN BEARINGS USING THIN-FILM STRAIN GAUGES

D. KONOPKA[*], T. STEPPELER[†], R. OTTERMANN[†], F. PAPE[*], F. DENCKER[†], G. POLL[*], M.C. WURZ[†]

[*] Institute of Machine Design and Tribology (IMKT)
Leibniz University Hannover
An der Universität 1, 30823 Garbsen, Germany
konopka@imkt.uni-hannover.de, www.imkt.uni-hannover.de

[†] Institute of Micro Production Technology (IMPT)
Leibniz University Hannover
An der Universität 2, 30823 Garbsen, Germany
steppeler@impt.uni-hannover.de, www.impt.uni-hannover.de

Abstract. The world's electrical energy demand is rising permanently and, at the same time, resources must be used economically and responsibly. An important part of the energy turnaround are wind mills, where conventional machine elements such as gears or rolling bearings find application. These parts have optimization potential in terms of service life and reliability. To advance this potential, sensor integration for intelligent system monitoring combined with a compact electronic solution has to be realized. In contrast to conventional condition monitoring systems (CMS), this article addresses thin-film sensors that will be applied inside the bearing system directly inside or close to the tribological contact enabling maximum information about the system's condition. For this purpose, thin-film strain gauges are directly deposited onto small steel bearing washers of a cylindrical roller thrust bearing system (CRTB) by photolithography and sputtering processes. The layer stack includes an aluminum oxide insulation layer, the sensor layer and an aluminum oxide wear protection coating. The sensor layer consists of an array of three differently aligned meander-shaped constantan strain gauges. Therefore, bearing washers with the sensors are tested on a pin-on-plate tribometer under defined load conditions. The influence of normal force as well as velocity on the thin-film sensors could be detected in this study. During the tests, under Hertzian pressure up to 1 GPa and a constant sliding velocity of 8 mm/s, a maximum nominal resistance change $\Delta R/R_0$ of up to -0.13 ‰ was measured. Changing the velocity from 1 mm/s to 8 mm/s resulted in maximum $\Delta R/R_0$ values of -0.17 ‰. This enables the determination of the correlation between sensor signals and tribological stresses. Though Hertzian pressures of 950 MPa were applied, no sensor failure was observed during the experiments proving the functionality of the sensor layer system.

Key words: Bearings, Thin-film sensors, Strain gauges, Tribological contact, Condition monitoring systems (CMS)

Peer-review under responsibility of the organizing committee of SMART 2023.
doi: 10.7712/150123.9934.443603

1 INTRODUCTION

The automation of machines is becoming increasingly important in today's world. An important aspect here is the integration of sensors in machine elements to enable continuous monitoring of operating states. In most cases, important measured variables such as strain and temperature are measured with the help of resistive sensors. Metallic strain gauges are used in the automotive industry to measure strain as well as pressure condition of castings and engine blocks [1]. In the energy sector, temperature and strain sensors are used to quantitatively evaluate the structural performance of buried pipelines considering longitudinal bending loads and axial thermal stresses [2]. There are several approaches that can be used for higher-level monitoring of machine components such as bearings. These aim to prevent damage to the bearing caused by complex conditions such as heavy loading and high speed over a long period of time [3].

In the coming years, there is a growing need to continuously monitor the performance of machine elements, such as bearings, over extended periods and analyze their operating conditions. This is essential to prevent unplanned downtimes caused by excessive vibrations or temperature fluctuations in machines, and to improve maintenance intervals for better efficiency and productivity. Using direct-deposited strain and temperature sensors fabricated directly on the surface of the bearing washer at the location of the elastohydrodynamic lubrication (EHL) in rolling contact, to determine the elasto-plastic deformations and contact condition. Because of their small thickness of a few micrometers [4], these sensors can generate data at previously inaccessible measurement locations [5]. They have a high adhesion to steel, withstand temperatures up to 400 °C [6] and can be applied and structured on curved surfaces as well [7].

The IMKT achieved first experimental results of thin-film sensors inside the rolling contact of a bearing. First measurement values of the contact pressure and temperature were recorded in the EHL contact [8,9]. Another concept of integrated sensor systems in the rolling contact is presented by Gao et al. The aim was to record the operating conditions. The sensors were able to measure tribological information, such as contact pressure and vibration, and communicate in real time with a measurement computer [10]. Furthermore, thin-film strain sensors have already been used to measure rolling contact loads on axial cylindrical roller bearings (CRTB) washers. The sensitivity of the system was 4.08 mV/kN [11].

For this study, a CRTB is used where the sensors can be applied on the flat surface of the bearing washer. Figure 1 shows the components of the bearing and schematically the conversion of the mechanical stress to a resistance change by means of strain gauges. It is also necessary to mention that the tests are carried out under simplified conditions to verify the concept and manufacture of a sensor. Therefore, an oscillating tribometer is used. For this reason, the sensor positions produced are arranged linearly. In the later project stages, the concept will be scaled to larger rolling bearings. The sensor system consists of an insulation layer of aluminum oxide (Al_2O_3), followed by the strain gauges of constantan ($Cu_{54}Ni_{45}Mn_1$), the supply lines of gold and finally an insulation and wear protection layer of Al_2O_3. This

sensor array is subjected to oscillating loads with different forces and speeds. Meanwhile, the sensor signal is recorded.

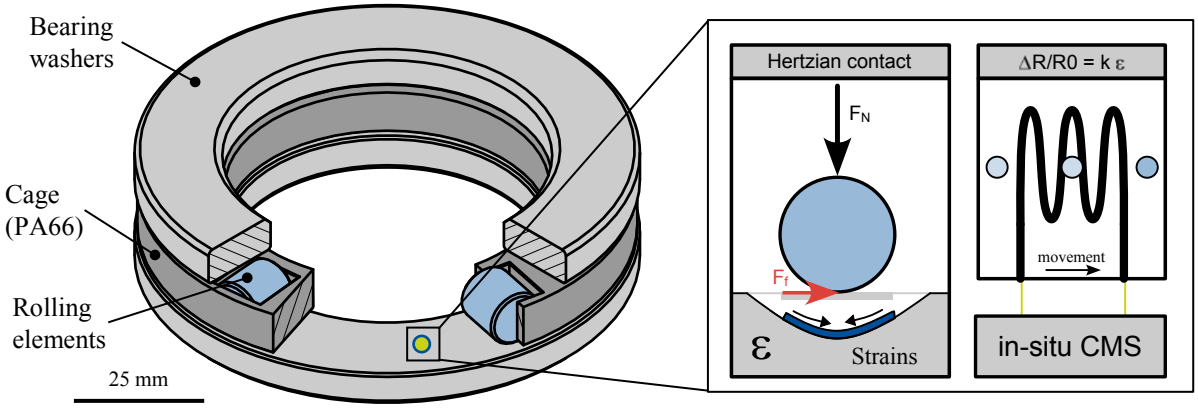

Figure 1: Schematic illustration of the planned tribological system (CRTB 81212) and a view of the used sensor technology.

2 MATERIALS AND METHODS

In this section, the processes for fabricating the thin-film sensors on CRTB using cathode sputtering are described in detail.

2.1 Sensor design

The sensor design consists of three strain gauges (named 0°, 45° and 90°), each rotated by 45°. The strain gauges consist of ten parallel lines, each 10 µm wide, connected by meandering joints, giving a total length of 5 mm. Each sensor covers a total area of approximately 400 µm x 400 µm. The complete sensor system is shown in Figure 2.

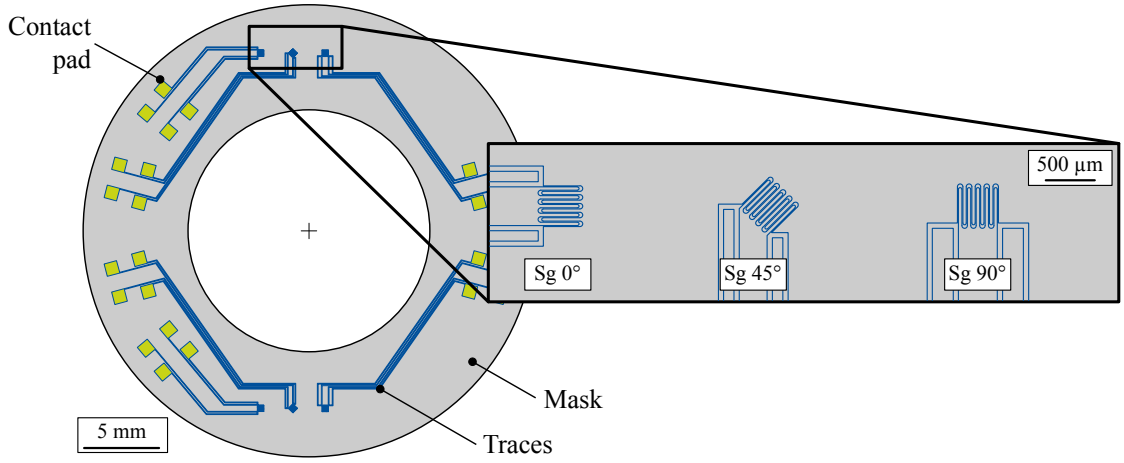

Figure 2: Mask design (left) and sensor array (right) with strain gauges Sg 0°, Sg 45° and Sg 90°

2.2 Sensor production

A bearing washer of the axial cylindrical roller bearing type 81102 from INA was used as the substrate for the thin-film sensors. The initial average roughness depth R_z was 0.698 ± 0.064 µm and the arithmetic mean roughness value R_a was 0.098 ± 0.008 µm, measured with a tactile perthometer (Mahr GmbH, Germany). At the beginning of the deposition of the insulation layer on the bearing washer, a sputter etching process was performed in a SenVac Z550 sputtering system to increase the adhesion strength of the subsequent insulation layer. The etching process was performed with a power of 200 W and a DC bias voltage of 117 V over a period of 5 minutes at a base pressure of $6.4 \cdot 10^{-5}$ mbar and a sputtering pressure of $3.3 \cdot 10^{-3}$ mbar in a pure argon atmosphere. Afterwards, the insulation layer of Al_2O_3 was deposited with a power of 400 W (1.88 W/cm²) at a base pressure of $7.4 \cdot 10^{-6}$ mbar and a process pressure of $3.2 \cdot 10^{-3}$ mbar. During the process, 85 sccm of argon and 3 sccm of oxygen were constantly supplied to the chamber. 4 µm thick insulating layer was deposited with a deposition rate of 8.3 nm/min. Subsequently, microengineering methods were used to fabricate the thin-film sensors with lift-off processes for patterning and deposition. After coating the substrate with AZ 5214 E resist, soft bake on a hot plate at 105 °C, exposure, post exposure bake on a hot plate at 120 °C and development, constantan strain gauges were sputtered using the SenVac Z550 system. A 500 nm thick film was generated with a power of 200 W and a process pressure of $3.8 \cdot 10^{-3}$ mbar in a pure argon atmosphere. The deposition rate was 10 nm/min. To reduce the trace resistance, a 500 nm thick layer of gold was deposited on the traces and the contact pad over a period of 25 min. For this purpose, the Kenotec MRC sputtering system was used with a power of 200 W, a base pressure of $2.4 \cdot 10^{-6}$ mbar and a sputtering pressure of $4.6 \cdot 10^{-3}$ mbar. Finally, a 4 µm Al_2O_3 was deposited as an anti-wear layer using the SenVac Z550 sputtering system and the previously described settings for deposition of the Al_2O_3 insulating layer. During this process, the contact pads were covered with a previously laser fabricated stainless-steel shadow mask

to ensure the subsequent contacting capability at the sensors' contact pads. Figure 3 shows the layer stack on the left side and a microscopic image of a sensor array on the right side.

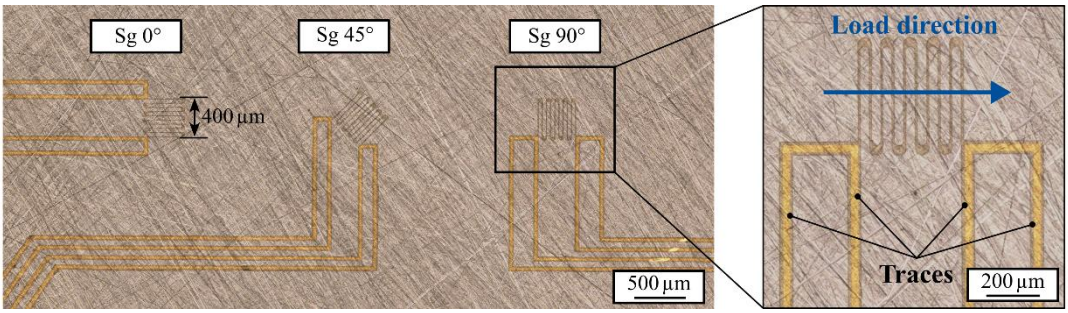

Figure 3: Microscopic image of a produced strain gauge array.

Due to the gold layer on the contact pads, it was possible to carry out the contacting by soldering. Thin wires led to contacting boards where cables of the measurement system could be inserted. A contacted bearing washer is shown in Figure 4.

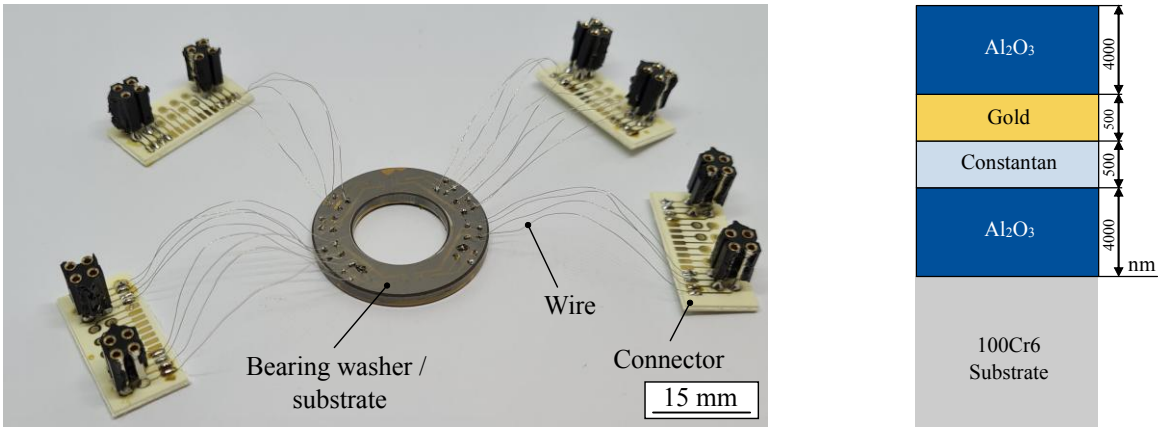

Figure 4: Overview of the produced sample: (a) Bearing washer with contacted thin-film sensors. (b) Schematic section view of the layer system of a trace (unscaled).

2.3 Test rig

A linear oscillating pin-on-plate tribometer was used for the investigations of the thin-film sensors so that a clearly defined setting is possible. In addition, this results in a clearer assignment of sensor signals to the settings. Likewise, the design of the contacting of the sensors is greatly simplified. The linear movement of the tribometer is realized by a step motor. Different geometries can be used as counter bodies. For this study, bearing balls made of 100Cr6 with a diameter of 6 mm were selected. The ball is fixed in the sample holder. A sliding contact with 100% slip is therefore present. The linear raceway of the tribometer must be positioned exactly in the linearly arranged sensor array. A microscope was used for

positioning. In this way, all sensors were stressed after each other by the oscillating movement and the tribological contact. The tribometer allows various constant sliding speeds (up to 8 mm/s) and normal forces F_N (up to 3 N). The selected contact combinations enable Hertzian pressures p_H of up to 950 MPa. The lubricant used for the investigations is GLEITMO 585 K grease (Fuchs Lubricants GmbH, Germany).

During the test, the tangential force is determined and recorded by means of a displacement sensor. To illustrate the test, the oscillating motion is shown schematically in Figure 5.

To calculate the resistance changes (caused by strain), the time signal is analyzed and explained below. The counterbody moves from the start position to the turning point. This path is defined as stroke which has a length of 8 mm. After reaching the turning point, the ball returns to its initial position. Within the oscillating movement, the tribological contact stresses the sensors twice. For the measurement of the strain gauge resistances, 10 cycles per experiment are analyzed. For the investigations, the sensors are loaded with forces of 1 N (660 MPa), 2 N (830 MPa) and 3 N (950 MPa). Likewise, a variation of the velocity of 1 mm/s, 4 mm/s and 8 mm/s takes place. The systems are combined with a measuring amplifier QuantumXBox MX1615B (Hottinger Baldwin Messtechnik GmbH). Four-wire technology is used here to measure the pure sensor resistances excluding the resistance generated by wires, supply lines and contact points.

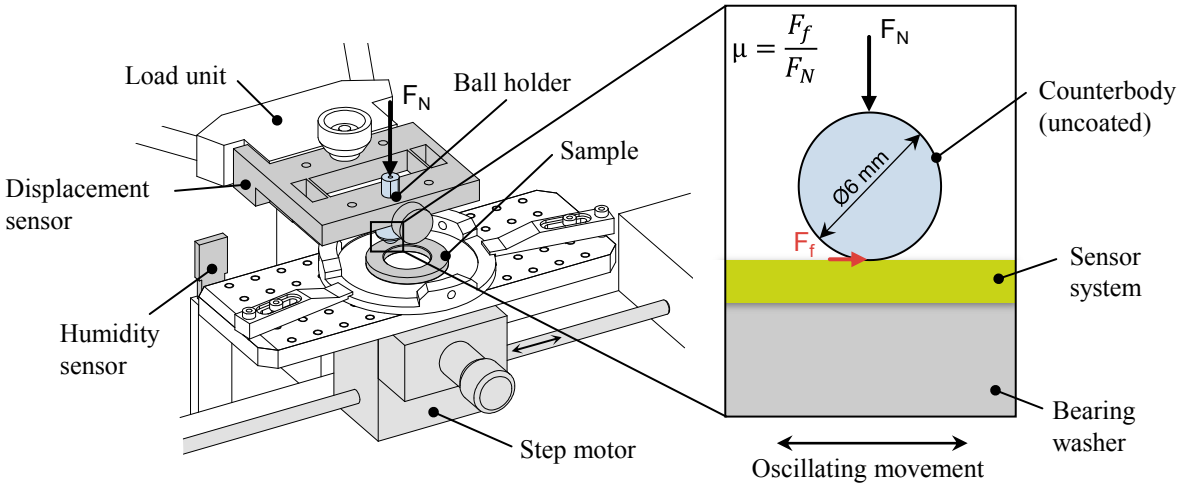

Figure 5: Schematic structure of the test rig that performs linear oscillating sliding movements of a steel ball on the bearing washer.

3 RESULTS

In this section, the determined changes in sensor resistance due to the tribological loads are analyzed and compared. In order to provide an overview of the events, the experiment with a normal force of 3 N and a sliding speed of 8 mm/s is described in more detail. In this

experiment, the tribological stresses are highest with respect to the Hertzian pressure p_H and the sliding speed v. Using this as an example, the resistance change is described and the tribological stress can be measured with time resolution.

The measurement of the signal from sensor Sg 45° resulted in contradictory resistances. On the one hand, the measured base resistance R_0 was significantly higher than the other two sensors, and on the other hand, the effective resistance change per cycle could not be reproducibly determined. The results of the measurements were therefore not taken into account, as it can be assumed that the sensor was already defective at the beginning of the tribological investigations.

Initially, the recorded 10 cycles from strain gauge Sg 90° and Sg 0° are resolved in time. In order to classify the effects and reactions of the signal, it should be noted again that Sg 0° is oriented directly to the sliding direction. The second sensor is rotated 90° and is arranged transversely within the raceway. Based on Figure 6, the uniform movement of the ball is visible, as well as the change in resistance of the respective sensors. The resistance of the sensor Sg 90° is shown on the left axis. The equivalent of Sg 0° is shown on the right vertical axis.

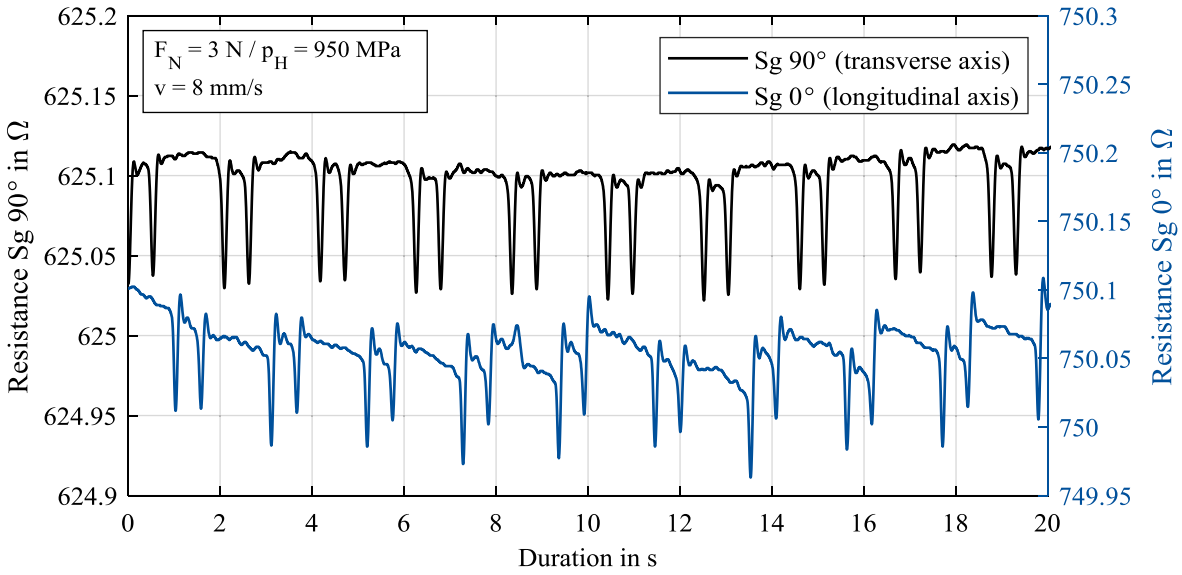

Figure 6: Measured resistance changes as a function of time of the sensors Sg 90° and Sg 0.

The focus is now on the Sg 90° signal. It can be seen that the local extrema of the black curve occur periodically. Due to the chosen experimental parameters of speed (8 mm/s) and a stroke of 8 mm, the time of one cycle is 2 s. With the background that the oscillating motion stresses the respective sensor twice within one cycle, another reaction per cycle is to be expected and can be seen in the diagram. When considering the cumulative signal course, the experiment with 10 cycles lasts 20 s. At the same time, the resistances of Sg 0° were recorded. The local extrema and reactions of the signal course (see blue curve) also show periodically recurring signals. In each cycle, there is a negative signal drift that cannot be explained so far. Further investigations have to be carried out. It might be due to the used grease, which is

redistributed into the mechanical contact by the continuous oscillation. It should be noted that the nominal resistance values of the sensors are different (625.1 Ω for Sg 90° and 750.05 Ω for Sg 0°).

To eliminate this effect from the measurement data and to better compare the measurements with each other, the normalized resistance changes $\Delta R/R_0$ must be calculated. This value indicates the effective resistance change per cycle and generally describes the compression and elongation of a strain gauge. For the produced strain gauges, the characteristics were determined in previous investigations under tensile loads, and the *k*-factor was determined to 2.15 [14]. It indicates the proportionality of the resistance change ΔR to the strain ε. This allows the calculation of the measured resistances to strain. To do this, the base resistance before the sensor is subjected to stress is determined and subtracted from the extreme value of each cycle. If the calculated value ΔR is negative, compression can be assumed. An increase in elongation or stretching is expected if the value is positive. Using this approach, the effective resistance change was determined and evaluated for each cycle. Particularly in Figure 6, it is evident that the recurring periods and extreme points are comparable and reproducible. However, to examine a cycle in more detail, Figure 7 shows the normalized resistance change $\Delta R/R_0$ for the time from 15 s to 19 s from Figure 6 (3 N and 8 mm/s). In the signal of Sg 90°, reproducible resistance changes of up to -0.13 ‰ can be observed during the time when the sensor is subjected to mechanical contact. This corresponds to an effective strain per cycle of about -60 µm/m.

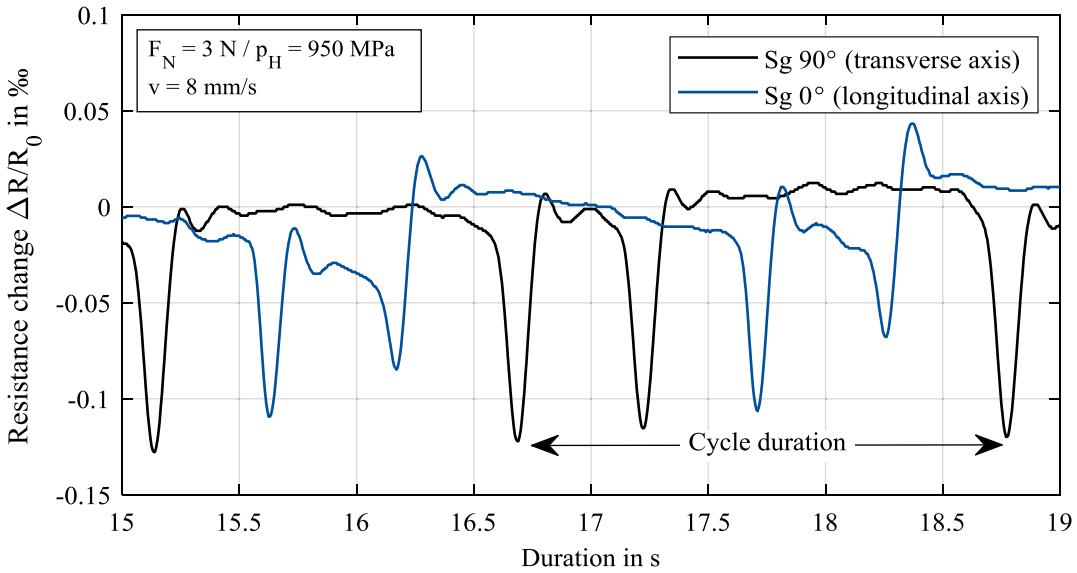

Figure 7: Normalized resistance change with focus on a cycle.

It is positive to note that the expected tribological stresses were resolved in spatial and temporal and the resistance changes could be detected in both sensors. In addition to the aforementioned compressions, elongations can be observed immediately after the ball passes over the longitudinal strain gauge. These reactions are theoretically and simulatively explained in [12] due to the elastic deformation with alternating compression and elongation

of the Hertzian contact in horizontal direction during the passage of the ball, and could be detected here. The comparison of the two sensor signals shows that the primary resistance changes were measured in the same direction and this was caused by the dominant normal force. From a tribological point of view, the reaction on the surface is a combined force in the normal and also in tangential directions. This is evident especially in the measurement of the sensor Sg 0°. Here, the positive resistance changes are clearly visible after each negative resistance change. This can be explained by [12].

In this study, in addition to the functionality of the sensors, a correlation between Hertzian pressure p_H and sliding velocity v was to be established for the stress on the sensor. To this end, an overview of various experiments is presented in Figure 8. For each individual experiment, 10 cycles were evaluated and the respective normalized resistance change $\Delta R/R_0$ was determined. Here, the mean values and the corresponding standard deviations are plotted. Figure 8a shows the resistance change as a function of Hertzian pressure at constant sliding velocity (8 mm/s). It is trending apparent that increasing the contact pressure triggers a higher effect on the sensors. Both sensors (Sg 90° and Sg 0°) qualitatively measure similar resistance changes which shows that the main cause for the signals is the normal force and not a tangential force.

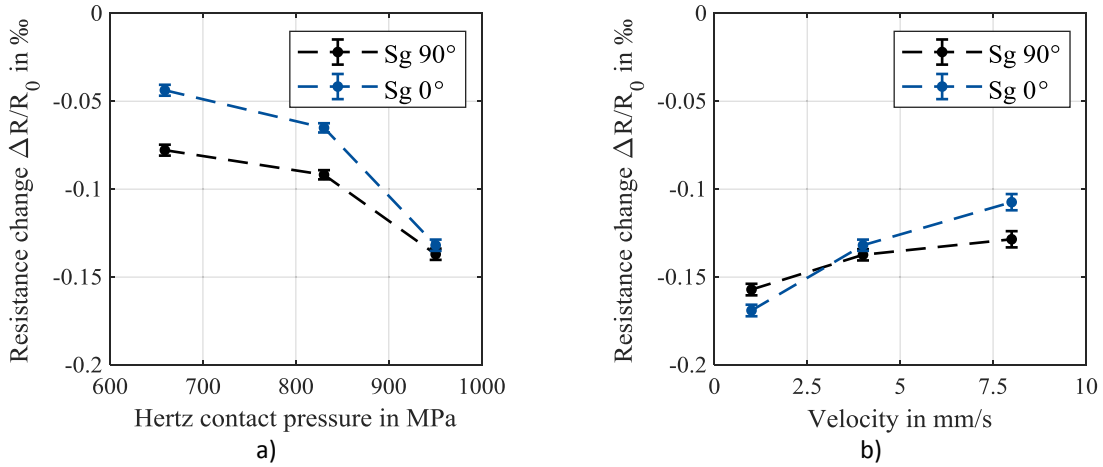

Figure 8: Comparison of resistance changes: (a) Constant sliding velocity (8 mm/s). (b) Constant Hertzian pressure (950 MPa).

In Figure 8b, the experiments were performed at a constant Hertzian pressure (950 MPa) with varying sliding velocities (1 mm/s, 4 mm/s and 8 mm/s). The results show that lower sliding velocities lead to higher stress on the sensor. This could be because at higher velocities the film thickness is sufficiently developed, and the solid contact fraction is lower. However, at very low sliding velocities in an oscillating motion, the lubricant may not effectively separate the tribological partners, and the play between static and dynamic friction can cause a stick-slip effect, resulting in increased shear strains.

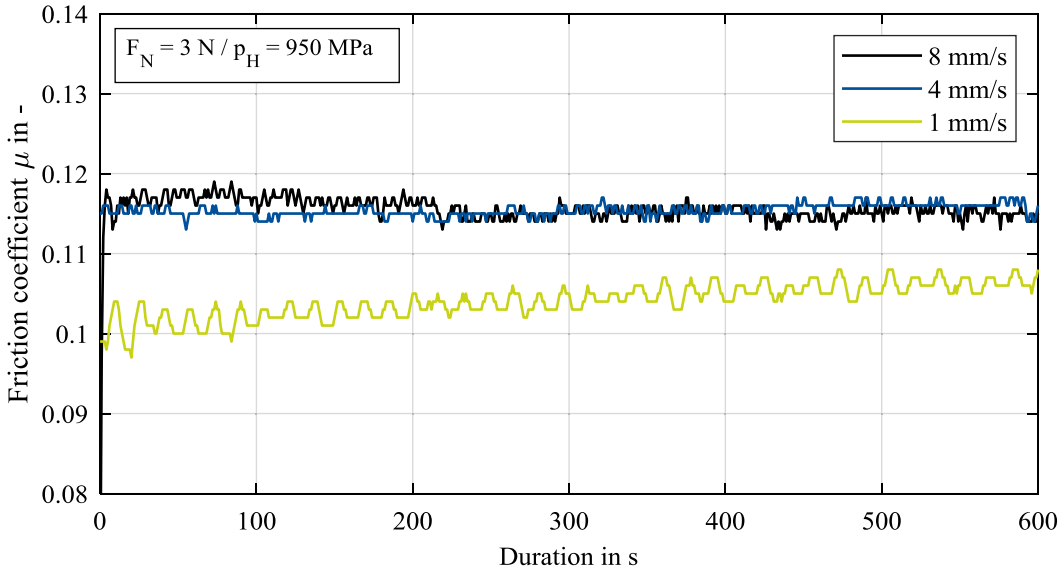

Figure 9: Comparison of the coefficient of friction under constant Hertzian pressure and various sliding speeds.

The experiments also yielded a quantitative coefficient of friction of 0.112 ± 0.005, which is consistent with the previous experiments by [13]. However, the stick-slip effect was not adequately resolved with the current measuring tools. The analysis of the friction coefficient recordings at a constant Hertzian pressure of 950 MPa and different sliding velocities, analogous to Figure 9, revealed larger amplitudes around the mean value. These are caused by the constant acceleration and deceleration within the oscillatory motion and confirm the effect of stick-slip at low frequency.

4 SUMMARY AND OUTLOOK

In this study, results of an oscillating load applied by a linearly moving ball on sputtered thin-film constantan strain gauges embedded in an Al_2O_3 layer for insulation and wear protection on cylindrical roller thrust bearing washers were presented. The applied force causes a compression which changes the sensor signal. The focus in this work was placed on two specific strain gauges that were oriented parallel (Sg 0°) and perpendicular (Sg 90°) to the oscillating movement of the ball. The results show that the expected tribological stresses could be spatially and temporally resolved and the change in resistance could be detected in both sensors. This proves the general functionality of the thin-film system in tribological contact. At a constant velocity of 8 mm/s and increasing normal force, the sensors experienced increasing nominal resistance changes $\Delta R/R_0$ with a maximum of -0.13 ‰ which corresponds to a strain of -60 µm/m. Even though the alignment of the strain gauges was perpendicular to each other, the signals showed a similar behavior in general. The reason for this is the normal force exerted by the ball. Where the normal force acts, the bearing disc behaves like a membrane and is minimally compressed. This causes the strain gauges to be

compressed (negative strain), which results in a reduction in resistance. In addition, positive strain was also detected immediately after the ball passed over the Sg 0° sensor. These reactions are explained theoretically and numerically in [12] due to the elastic deformation with alternating compression and elongation of the Hertzian contact during the passage of the ball because of tangential forces and could be verified here.

In summary, this article shows the general functionality of thin-film strain gauges with the presented layer stack and the influence of different normal forces and velocities of a linear pin-on-plate tribometer.

In the future, also a temperature sensor will be implemented in this sensor system to measure temperature changes due to the tribological contact, especially without lubrication. Over the entire test period of this study, no wear could be detected on the surface of wear protection layer. Therefore, further tests will be carried out over a longer period of time in order to be able to analyze the service life of the wear protection layer made of Al_2O_3. Additional research should also be conducted on rolling contact, as the implementation of this sensor system in rolling bearings aims to identify critical load conditions like overloading or inadequate lubrication.

4 ACKNOWLEDGMENTS

The authors thank the German Research Foundation (DFG) that funded this work within the research project “Integrated sensors for intelligent large-diameter bearings” (project number 466778958) as part of the Priority Program 2305 “Sensor-integrating machine elements” (project number 441853410).

REFERENCES

[1] Sediako, D.; Stroh, J.; Kianfar, S. Residual Stress in Automotive Powertrains: Methods and Analyses. Materials Science Forum 2021, 1016, 1291–1298. https://doi.org/10.4028/www.scientific.net/MSF.1016.1291.

[2] Feng, X.; Han, Y.; Wang, Z.; Liu, H. Structural performance monitoring of buried pipelines using distributed fiber optic sensors. Journal of Civil Structural Health Monitoring 2018, 8, 509-516. https://doi.org/10.1007/s13349-018-0286-3

[3] Chen, X.F.; Wang, S.B.; Qiao, B.J.; Chen, Q. Basic research on machinery fault diagnostics: Past, present, and future trends. Frontiers of Mechanical Engineering 2018, 13, 264–291. https://doi.org/10.1007/s11465-018-0472-3.

[4] Ottermann, R.; Klaas, D.; Dencker, F.; Hoheisel, D.; Rottengatter, P.; Kruspe, T.; Wurz, M.C. Direct Deposition of Thin-Film Strain Gauges with a New Coating System for Elevated Temperatures. In Proceedings of the IEEE Sensors, Rotterdam, The Netherlands, 25–28 October 2020; pp. 1–4. https://doi.org/10.1109/SENSORS47125.2020.9278661.

[5] Heikebrügge, S.; Ottermann, R.; Breidenstein, B.; Dencker, F.; Wurz, M.C. Residual stresses from incremental hole drilling using directly deposited thin film strain gauges. Exp. Mech. 2022, 62, 701–713. https://doi.org/10.1007/s11340-022-00822-0.

[6] Klaas, D.; Ottermann, R.; Dencker, F.; Wurz, M.C. Development, Characterisation and High-Temperature Suitability of Thin-Film Strain Gauges Directly Deposited with a New Sputter Coating System. Sensors 2020, 20, 3294. https://doi.org/10.3390/s20113294.

[7] Ottermann R., Klaas D., Dencker F., Hoheisel D., Jung S., Wienke A., Duesing J.F., Koch J., Wurz M.C. Directly Deposited Thin-Film Strain Gauges on Curved Metallic Surfaces. In Proceedings of the IEEE Sensors, Sydney, Australia, 31 October–4 November 2021; pp. 1–4. https://doi.org/10.1109/SENSORS47087.2021.9639542.

[8] Schmidt U., "Die Schmierfilmbildung in elastohydrodynamischen Wälzkontakten unter Berücksichtigung der Oberflächenrauheit", Thesis, Leibniz University Hanover, 1985.

[9] Bauerochs R., "Druck- und Temperaturmessungen in EHD - Wälzkontakten", Thesis, Leibniz University Hanover, 1989.

[10] Gao R., Holm-Hansen B., Wang C. Design of a mechatronic bearing through sensor integration, Proc. SPIE 3518, Sensors and Controls for Intelligent Machining, Agile Manufacturing, and Mechatronics, 1998, doi: 10.1117/12.332801.

[11] Winkelmann C., Woitschach O., Meyer E.-M., Lang W. Development of a strain sensor for rolling contact loads. International Solid-State Sensors, Actuators and Microsystems Conference, Beijing, China, 05-09 June 2011; DOI: 10.1109/TRANSDUCERS.2011.5969179

[12] Meyer C., Reibung in hoch belasteten EHD-Wälzkontakten, Dissertation, Uni Hannover, 2010

[13] Konopka D., Pape F., Ottermann R., Steppeler T., Dencker F., Wurz M.C., Poll G. Characterization of an anti-wear coating for the application of highly loaded smart thin-film sensors. In Proceedings of the International Scientific Conference BALTTRIB 2022, Kaunas, Lithuania, submitted, 2022

[14] Ottermann, R.; Steppeler, T.; Dencker, F.; Wurz, M.C. Degeneration Effects of Thin-Film Sensors after Critical Load Conditions of Machine Components. *Machines* 2022, *10*, 870. https://doi.org/10.3390/machines10100870